

AperTO - Archivio Istituzionale Open Access dell'Università di Torino

Energy metabolism in osteoclast formation and activity

This is the author's manuscript

Original Citation:

Availability:

This version is available <http://hdl.handle.net/2318/1657307> since 2018-01-12T18:24:01Z

Published version:

DOI:10.1016/j.biocel.2016.08.034

Terms of use:

Open Access

Anyone can freely access the full text of works made available as "Open Access". Works made available under a Creative Commons license can be used according to the terms and conditions of said license. Use of all other works requires consent of the right holder (author or publisher) if not exempted from copyright protection by the applicable law.

(Article begins on next page)

Energy metabolism in osteoclast formation and activity

Silvia Lemma^{a,b}, Martina Sboarina^c, Paolo E. Porporato^c, Nicoletta Zini^{d,e}, Pierre Sonveaux^c,
Gemma Di Pompo^a, Nicola Baldini^{a,b}, Sofia Avnet^a

^a *Orthopaedic Pathophysiology and Regenerative Medicine Unit, Istituto Ortopedico Rizzoli, via di Barbiano 1/10, 40136 Bologna, Italy*

^b *Department of Biomedical and Neuromotor Sciences, University of Bologna, 40136 Bologna, Italy*

^c *Pole of Pharmacology, Institute of Experimental and Clinical Research (IREC), Université catholique de Louvain (UCL) Medical School, Brussels 1200, Belgium.*

^d *CNR – National Research Council of Italy, Institute of Molecular Genetics, 40136 Bologna, Italy*

^e *Laboratory of Musculoskeletal Cell Biology, Istituto Ortopedico Rizzoli, 40136 Bologna, Italy*

Corresponding author: Sofia Avnet, PhD, Orthopaedic Pathophysiology and Regenerative Medicine Unit, Istituto Ortopedico Rizzoli (IOR), via di Barbiano 1/10, 40136 Bologna, Italy. E-mail: sofia.avnet@ior.it

Short (page heading) title: Energy metabolism in osteoclast formation and activity

A B S T R A C T

Osteoclastogenesis and osteolysis are energy-consuming processes supported by high metabolic activities. In human osteoclasts derived from the fusion of monocytic precursors, we found a substantial increase in the number of mitochondria with differentiation. In mature osteoclasts, mitochondria were also increased in size, rich of cristae and arranged in a complex tubular network. When compared with immature cells, fully differentiated osteoclasts showed higher levels of enzymes of the electron transport chain, a higher mitochondrial oxygen consumption rate and a lower glycolytic efficiency, as evaluated by extracellular flux analysis and by the quantification of metabolites in the culture supernatant. Thus, oxidative phosphorylation appeared the main bioenergetic source for osteoclast formation. Conversely, we found that bone resorption mainly relied on glycolysis. In fact, osteoclast fuelling with galactose, forcing cells to depend on Oxidative Phosphorylation by reducing the rate of glycolysis, significantly impaired Type I collagen degradation, whereas non-cytotoxic doses of rotenone, an inhibitor of the mitochondrial complex I, enhanced osteoclast activity. Furthermore, we found that the enzymes associated to the glycolytic pathway are localised close to the actin ring of polarised osteoclasts, where energy-demanding activities associated with bone degradation take place. In conclusion, we demonstrate that the energy required for osteoclast differentiation mainly derives from mitochondrial oxidative metabolism, whereas the peripheral cellular activities associated with bone matrix degradation are supported by glycolysis. A better understanding of human osteoclast energy metabolism holds the potential for future therapeutic interventions aimed to target osteoclast activity in different pathological conditions of bone.

Keywords: osteoclast, energy metabolism, mitochondria, glycolytic efficiency, differentiation.

Abbreviations: ATP, Adenosine Triphosphate; M-CSF, Macrophage Colony-Stimulating Factor; RANKL, Receptor Activator of Nuclear Factor-Kappa B Ligand; OxPhos, Oxidative Phosphorylation; TCA Cycle, Tricarboxylic Acid Cycle; NF-kB, Nuclear Factor-Kappa B; PGC-1 β , Peroxisome Proliferator-Activated Receptor- Γ Coactivator 1 β ; V-AtPases, Vacuolar H(+)-ATPases; PBMC, Peripheral Blood Mononuclear Cells; TRAP, Tartrate-Resistant Acid Phosphatase; HSP60, Heat Shock Protein 60 KDa; GAPDH, Glyceraldehyde 3-Phosphate Dehydrogenase; PKM2, Pyruvate Kinase Isozymes M2; OCR, Oxygen Consumption Rate; ECAR, Extracellular Acidification Rate; FCCP, Carbonyl Cyanide 4-Trifluoromethoxy Phenylhydrazone; mtOCR, Mitochondrial OCR; ROI, Region Of Interest; mtDNA, Mitochondrial DNA; PI, Propidium Iodide.

1. Introduction

The skeleton is a metabolically dynamic tissue that undergoes continuous remodelling during life. Bone homeostasis is maintained by a delicate balance between deposition and resorption that is mediated by osteoblasts and osteoclasts that form and degrade bone, respectively (Teitelbaum, 2000). Pathological increases in osteoclast activity induce trabecular bone erosion which can result in various diseases, such as rheumatoid arthritis (Sweeney and Firestein, 2004), Paget's disease of bone (Erzurumlu et al., 2013), primary (Teitelbaum, 2000) or secondary laminopathies-associated osteoporosis (Zini et al., 2008), and osteolysis associated with cancer bone metastasis (Avnet et al., 2008).

Osteoclasts are giant, multinucleated, not-proliferative bone resorbing polykaryons that are formed by the differentiation and fusion of hematopoietic precursors of the monocytic and macrophagic lineage (Massey and Flanagan, 1999). Induction towards the osteoclast lineage is achieved through two essential cytokines, macrophage colony-stimulating factor (M-CSF) (Boyle et al., 2003) and receptor activator of nuclear factor-kappa B (NFkB) ligand (RANKL) (Blair et al., 2007, Novack, 2011). These and other pro-osteoclastogenic factors are locally produced by osteoblasts and other cells of bone microenvironment (Cenni et al., 2006, Granchi et al., 2004, Granchi et al., 2005). Interestingly, beside proteic factors, a reduced oxygen tension is also able to strongly induce osteoclast formation and function in different osteolytic conditions associated with hypoxia, such as osteoporosis, giant cell tumor of bone, and rheumatoid arthritis (Knowles and Athanasou, 2009, Knowles et al., 2010, Morten et al., 2013, Utting et al., 2010). Oxygen availability dictates the metabolic profile of living cells that, in turn, possibly modulates osteoclast formation and activation. In bone tissue, a correlation between metabolism regulation and cell differentiation has already been described. As an example, in osteoblasts, changes in metabolic pathways have been observed during their differentiation with glycolysis and

respiration continuously shifting one to the other in a delicate balance to support the different energetic demands during sequential differentiation stages (Komarova et al., 2000). In osteoclasts, similarly, high metabolic activity might be required for the energy-demanding steps of the differentiation process, including migration, fusion, actin reorganization, acid degradation and enzymatic activities for bone resorption. A few previous reports on osteoclasts derived from rats (Baron et al., 1986), from mice (Miyazaki et al., 2012) or from a murine myeloid cell line (Czupalla et al., 2005) showed that osteoclasts are mitochondria-rich cells with high expression of tricarboxylic acid cycle (TCA) and oxidative phosphorylation (OxPhos) enzymes. Moreover, intact and active mitochondria are required for osteoclast differentiation (Indo et al., 2013, Jin et al., 2014, Morrison et al., 1998). However, the basal metabolism of mouse and tumor cells is quite different from that of normal human cells. Indeed, metabolic enzymatic activities might significantly differ between mice and humans since murine cells have a lower metabolic stability (Demetrius, 2006). Regarding the osteoclast model that derives from murine myeloid cells, tumor cells are also notoriously more glycolytic than normal cells as a consequence of the Warburg effect (Pavlova and Thompson, 2016) and, therefore, are not the optimum model to study the metabolism of normal cells.

In this study, by using an in vitro models from peripheral blood precursors, for the first time we performed a comprehensive analysis of bioenergetics in human osteoclasts during their differentiation and function.

2. Methods

2.1. Human osteoclast cultures

Primary cultures of osteoclasts were obtained from monocytic precursors isolated from fresh buffy coats obtained from 15 different healthy volunteers (AVIS, Bologna, Italy; Saint-

Luc University Hospital, Brussels, Belgium), as previously described (Avnet et al, 2011). Buffy coats obtained from AVIS in Italy were collected after their expiration date (1 days after harvesting), whereas for buffy coats obtained from Saint-Luc University Hospital, Belgium, cells were isolated immediately after harvesting and after the ethical committee approval was obtained. Briefly, peripheral blood mononuclear cells (PBMC) were layered over Hystopaque (GE Healthcare) and seeded on tissue-culture glass or plasticware (3,000,000 cells/cm²) in DMEM (Sigma) supplemented with 25 mM glucose (Merck), 10% heat-inactivated characterized FBS (Celbio), plus 20 U/mL penicillin, 100 mg/mL streptomycin (Euroclone), and incubated at 37 °C in a humidified 5% CO₂ atmosphere. All experiments were performed in pyruvate- and glutamine-free media buffered at pH 7.4 (3.7 g/liter NaHCO₃) (complete DMEM), unless stated otherwise. After 2 hours, medium was discarded and replaced with complete DMEM added with RANKL [50 ng/mL] and M-CSF [10 ng/mL] (Peprotech) (pro-osteoclastogenic medium), or with complete DMEM without pro-osteoclastogenic factors (control medium), depending on the experimental conditions. In order to verify osteoclast differentiation, after 5 to 7 days of cell culture, cells were analyzed for tartrate-resistant acid phosphatase (TRAP) activity by cytochemistry (Acid Phosphatase Leukocyte assay, Sigma) and stained with Hoechst 33258. Only TRAP+ cells with 3 or more nuclei were considered as osteoclasts. The quantification of osteoclast formation was obtained by counting the total number of osteoclasts in 6 random optical fields (20 x lens). The experiment was repeated with cells obtained from three different donors.

2.2. Immunofluorescence assays

Immunofluorescence assays were performed on PBMC cultured on glass coverslips with pro-osteoclastogenic medium or control medium. Cells were fixed in 2%

paraformaldehyde. Permeabilization was performed with 0.5% Triton X-100 in HEPES and blocked with 1% BSA. We used anti-mitochondria MAb against the surface of intact mitochondria (clone 113-1, MAB1273, Merck Millipore, 1:50), anti- Pyruvate kinase isozymes M2 (PKM2) polyclonal antibody (Cell Signaling, 1:200); and anti-glyceraldehyde 3-phosphate dehydrogenase (GAPDH) MAb (Santa Cruz, 1:50). As secondary antibodies we used anti-mouse or anti-rabbit antibodies Alexa Fluor 488 nm (Life Technologies). For the staining of polymeric actin (F-actin) we used phalloidin-TRITC (Sigma, 0.5 µg/mL). Nuclei were stained with Hoechst 33258. Mitochondrial mass index was quantified as the ratio of the area with a fluorescent signal to the total area of the single cell by using NIS Element image software BR4.00.00 (Nikon). Cells were counted in 28 different random fields. Mitochondria networks were observed by confocal microscope (Nikon TI-E).

2.3. *Electron microscopy*

CD14⁺ cells were isolated from the mononuclear cell population obtained from buffy coats with the method described above and according to the previously described protocol (Avnet et al., 2013). We used an immunomagnetic cell separation technique (MACS, Miltenyi Biotec). Cells were washed with MACS buffer (PBS pH 7.2 supplemented with 0.5 % BSA and 2 mM ethylene diamine tetracetic acid), and clumps were removed by passing cells through a 30 µm pre-filter. Cells were then centrifuged at 400 x g. The cell pellet was resuspended in MACS buffer and counted. 10⁷ cells were mixed with anti-CD14 MACS antibody-coated microbeads, and incubated at room temperature. The cell suspension was applied to an LS-positive selection column previously washed with MACS buffer, and placed in a magnetic separation unit. The column was rinsed and removed from the magnetic separation unit, and positive bound cells were flushed. The collected cell population was then used for ultrastructural analysis. Pellets of CD14⁺ cells from

PBMC and glass-adherent osteoclasts were fixed in 2.5% glutaraldehyde in 0.1 M cacodylate buffer, pH 7.4, for 1 hour, postfixed with 1% osmium tetroxide (Electron Microscopy Science), dehydrated in a graded series of ethanol, and embedded in Epon (Electron Microscopy Science). The embedded samples were sectioned by an ultramicrotome (Ultracut E, Richert-Jung, Leica Microsystem). Thin sections (90 nm thick) were collected on 300 mesh nickel grids and stained with uranyl acetate (Electron Microscopy Science) and lead citrate. Samples were observed by using a Zeiss EM 109 apparatus (Zeiss). Images were captured with Nikon digital camera Dmx 170 1200F and ACT-1 software.

2.4. Western blotting

PBMC were seeded on cell culture dishes, and maintained in pro-osteoclastogenic medium or control medium until osteoclast differentiation was obtained. When multinucleated TRAP⁺ cells were formed (around 7 days), cells were lysed with RIPA buffer [Tris pH 7.6 50 mM, NaCl 150 mM, Triton-X 100 5%, sodium deoxycholate 0.25%, EGTA pH 8 1 mM, NaF 1 mM] (Sigma) containing protease and phosphatase inhibitor cocktails (Roche). Protein lysates were subjected to reducing SDS-PAGE on polyacrylamide gel and transferred to nitrocellulose membrane (Thermo Fisher Scientific). Membranes were stained with Ponceau red (Sigma) to confirm equal amount protein loading. Blots were probed with MitoProfile Total OxPhos human antibody Cocktail (1:300, ab110411, Abcam), and with anti-Heat Shock Protein 60 kDa (HSP60, 1:2000, HPA001523, Sigma), followed by horseradish peroxidase-conjugated anti-mouse and anti-rabbit (GE Healthcare). To detect heat shock protein 60 (HSP60) within the same blot, nitrocellulose membranes were stripped with Restore Western Blot Stripping buffer (Thermo Fisher Scientific), and reprobed. The reaction was revealed by a

chemiluminescence substrate (ECL Western Blotting Detection Reagents, GE Healthcare). The signal from each band was quantified by dedicated software for densitometric evaluation (VisionWorksLS Analysis Software, Biospectrum, UVP). The experiment was repeated with cells obtained from four different donors.

2.5. ATP assay

PBMC were seeded on 12-well plate or on dentin slices on 96-well plate, and maintained in pro-osteoclastogenic medium or control medium until multinucleated TRAP+ cells were obtained (around 7 days on plastic, or 14 days on dentin). Two hours before the assay, media were changed with fresh pro-osteoclastogenic medium or control medium. Cells were washed and lysed by using boiling ATP lysis buffer [0.1 M Tris(hydroxymethyl) aminomethane (Tris base) (Sigma) and 2 mM EDTA adjusted to pH 7.75 with acetic acid (Sigma)]. Cell lysates were added to a reaction mixture containing luciferase and luciferine (ATP Determination Kit, Molecular Probes) for bioluminescence quantification by using Infinite® 200 PRO plate reader (Tecan). ATP level was normalized to total protein content (Bradford protein assay). The experiment was repeated with cells obtained from three different donors, with 4 technical replicates each.

2.6. Oxygen consumption and extracellular acidification measurement

Oxygen consumption rate (OCR) and extracellular acidification rate (ECAR) were determined using a Seahorse XF96 extracellular Flux analyzer with a mitostress kit (Seahorse Biosciences). PBMC were seeded on XF96 cell culture plate in control media or pro-osteoclastogenic medium, and incubated from 2 to 14 days. Culture media were replaced by base medium (unbuffered DMEM supplemented with 25 mM glucose) 1 hour before measurements. Selective inhibitors were injected during the measurements to

achieve the final concentrations of oligomycin [2 μ M], Carbonyl cyanide 4-trifluoromethoxy phenylhydrazone FCCP [0.9 μ M], rotenone [1 μ M] antimycin A [1 μ M], and 2-deoxy-glucose [100 mM]. Mitochondrial OCR (mtOCR) was assayed by injecting rotenone and antimycin A to acutely inhibit mitochondrial-driven oxygen consumption. mtOCR was calculated by subtracting non-mitochondrial OCR from total OCR levels. ATP coupling (mitochondrial respiration associated with cellular ATP production) was calculated by subtracting total OCR from OCR measured after the addition of Oligomycin. Indeed, Olygomycin blocks OxPhos-dependent ATP synthesis from oxygen consumption. Data were normalized for total protein content using the Bradford protein assay. The experiment was repeated with cells obtained from three different donors, with 7 technical replicates each.

2.7. Glucose consumption and lactate production

Glucose consumption and lactate production were measured by analysing the metabolite content of deproteinized cell culture supernatants. PBMC were seeded as described above on 96-well plates in control medium or pro-osteoclastogenic medium and cultured until multinucleated TRAP⁺ cells were formed (around 7 days). Media were then replaced by fresh medium at the respective condition, and after additional 5 days, the supernatants were collected. Metabolite concentrations were quantified using specific enzymatic assays on a CMA600 analyzer (CMA Microdialysis AB). Glucose consumption and lactate production were normalized by total protein content using the Bradford protein assay (Bio-Rad). The experiment was repeated with cells obtained from three different donors, with 5 technical replicates for each condition.

2.8. Resorption assay

Resorption activity was measured by using the OsteoLyse bone resorption assay kit (Lonza). Cells were cultured in pro-osteoclastogenic medium until osteoclast differentiation (5 to 7 days), and then medium was replaced with specific media for 72 hours. In particular, we used DMEM supplemented with penicillin [20 U/mL] and streptomycin [100 mg/mL], 10% FBS, buffered at pH 7.4 with 3.7 g/liter NaHCO₃, plus 20 mM glucose (complete glucose medium), 20 mM galactose (Sigma) (complete galactose medium), or with complete galactose medium supplemented with rotenone (10 nM, Sigma). Supernatants were collected after 10 days and the fraction of Type I collagen degradation quantified by the emission of Europium-labelled collagen fragments via time-resolved fluorescence (Infinite® 200 PRO, Tecan, exc. 340 nm, ems. 615 nm). The experiment was repeated with cells obtained from two different donors, with 4 technical replicates for each condition.

2.9. Cell viability assay

Cell viability was assessed by the Alamar Blue test (Invitrogen), according to manufacturer's instructions. Cells were cultured in pro-osteoclastogenic media until osteoclast differentiation was obtained (7 days), and then media were replaced with complete galactose media added with rotenone (1 to 250 nM), or control media without rotenone, for 72 hours. The Alamar Blue solution was added (10% v/v) to cell culture. After incubation for 4 hours at 37 °C, the medium was transferred into another plate and the fluorescence was measured using a microplate fluorescence reader (Infinite® 200 PRO, Tecan), with an excitation wavelength of 490 nm and an emission wavelength of 530 nm. Results were normalized to total protein content (Bredford assay, Bio-Rad). The experiment was repeated with cells obtained from three different donors, with 2 technical replicates for each condition.

2.10. Necrotic osteoclast assay

Cells were cultured and maintained in pro-osteoclastogenic media or control media until osteoclast differentiation was obtained (around 7 days), and then media was replaced with complete galactose media added with rotenone (10 to 250 nM), or control medium without rotenone, for 72 hours. At the end of the incubation period, cells were stained with propidium iodide (PI, Invitrogen) for 15 minutes at room temperature. Then, the obtained samples were observed by fluorescence microscopy, and necrotic cells that were positive to PI (red) in 8 different random fields were counted. The experiment was repeated with cells obtained from two different donors, with 4 technical replicates for each condition.

2.11. Statistical analysis

Statistical analysis was performed using GraphPad Prism version 5.00 for Windows (GraphPad Software, San Diego California USA, www.graphpad.com). Due to the low number of observations, data were considered as not normally distributed. We used the nonparametric Mann-Whitney U test to evaluate the differences, and Spearman Rank correlation for the correlation analyses. Data were expressed as mean \pm standard error of the mean (SEM). *P* values less than 0.05 were considered as statistically significant.

3. Results

3.1. Mitochondrial mass increases along osteoclast differentiation

We obtained human osteoclasts from PBMC treated with the pro-osteoclastogenic factors RANKL and M-CSF. At 2 days, we observed undifferentiated mononuclear osteoclast precursors that, after 7 days of culture, fused together to form TRAP⁺ multinucleated osteoclasts (Fig. 1A). The number of fully differentiated osteoclasts was

maintained from 7 to 14 days (Fig. 1A). In mature osteoclasts, we found that the mitochondrial mass was markedly and significantly increased with respect to cells at 2 days of culture (Fig 1B and C *** $p < 0.0001$). We also found a positive correlation between mitochondria mass and the number of nuclei (Fig. 1D, $R^2 = 0.9122$, * $p = 0.0178$). These data suggest that multinucleated cells retain the mitochondrial mass of the cells of origin, as they need to keep the same level of energy production from mitochondrial activity.

To analyse mitochondria at different osteoclast differentiation phases by ultrastructural analysis, we used CD14+ cells isolated from the mononuclear cell fraction of PBMC before the seeding (Massey and Flanagan, 1999). This method allows obtaining a pure population of osteoclast precursors, thereby avoiding the contamination with macrophages and lymphocytes. Osteoclasts showed larger mitochondria that were also richer in cristae than their precursors (Fig. 1E). By confocal analysis, we observed that in fully differentiated osteoclasts mitochondria form a reticulum clustered at the perinuclear region that extends outward with a tubular appearance towards the peripheral basal domain of the cell (Fig 2 and 3).

3.2. Mitochondrial energy metabolism increases during osteoclast differentiation

We then verified if the increased mitochondrial content of differentiated osteoclasts was associated with increased OxPhos and mitochondrial metabolism. We therefore analyzed the expression of OxPhos complex subunits, the total intracellular content of ATP, and the respiration rate in osteoclasts with respect to immature cells (mononuclear precursors cultured for the same number of days and not treated with the osteoclast differentiating-factors RANKL and M-CSF). Western blotting revealed that osteoclasts expressed significantly higher levels of complexes I, II, III and V (Fig 4A-B; I-NDUFB8 * $p = 0.0495$, II-SDHB * $p = 0.095$, III-UQCRC2 * $p = 0.0339$, V-ATP5A * $p = 0.0495$) with respect to immature

cells. Furthermore, we found that mature osteoclasts produced higher levels of intracellular ATP when compared to undifferentiated cells (Fig 4C, ** $p=0.0089$; Fig 4D, *** $p=0.0001$). As a means of verification of the increased OxPhoS metabolism in human osteoclasts, we measured the oxygen consumption rate (OCR) and extracellular acidification rate (ECAR) of live fully differentiated cells with respect to immature cells under the same timing and conditions of those used for western blotting analysis. We found that ECAR values were always lower in cells treated with RANKL and M-CSF, and already at 2 days of culture, with respect to untreated cells (Fig. 5A). Conversely, OCR was higher in osteoclasts (cells treated with RANKL and M-CSF at 7 and 14 days of cultures) than in immature cells (cells not treated with RANKL and M-CSF the same time points) (Fig. 5B). By using ECAR and OCR measurements of different osteoclast cultures after 7 days of incubation, we calculated the rotenone and antimycin A-sensitive OCR (mtOCR) and the ATP coupling efficiency. We found a significantly higher mtOCR, with a trend towards increased ATP coupling and decreased ECAR in mature cells with respect to immature cells (Fig. 5C). ECAR is an indirect method to evaluate glycolytic activity. Therefore, we also measured the glycolytic efficiency as the ratio of lactase production/glucose consumption (Zancan et al., 2010). Consistently with the data obtained by extracellular flux analysis, we found a significantly lower glycolytic efficiency in cells treated with RANKL and M-CSF compared with untreated cells (Fig. 5D *** $p<0.0001$).

In conclusion, the high expression of subunits of the electron transport chain, the high intracellular ATP content, the increased OCR and the reduced glycolysis suggest an increased OxPhoS metabolism and a concomitant decrease of glycolysis during the differentiation of human osteoclasts.

3.5. Osteoclasts switch to a more glycolytic metabolism for Type I collagen resorption

After confirming that the energetic demand for osteoclast formation is largely fulfilled by an oxidative metabolism, we wondered whether the same energetic source and metabolism was also used during the bone resorption process. To this purpose, differentiated osteoclasts were exposed to complete cell culture medium containing only glucose or only galactose as energetic fuels (Kase et al. , 2013) and seeded on a layer of collagenous matrix. Compared to glucose, galactose forces cells to depend on OxPhos to generate sufficient ATP by reducing the rate of glycolysis (Weinberg et al. , 2010). We found that, when mature osteoclasts were exposed to glucose, Type I collagen degradation activity was significantly increased, whereas the addition of galactose to the cell medium significantly affected the resorption of collagenous matrix (Fig 6A; *p=0.0132). Furthermore, the combination of galactose with rotenone, a specific inhibitor of complex I of the electron transport chain significantly increased Type I collagen degradation activity with respect to cell cultures containing only galactose in the medium (Fig 6A, **p=0.0013). Of note, the 10 nM concentration of rotenone used for the Type I collagen resorption assay was not cytotoxic (Fig 6B and C). Altogether, our results demonstrated that glycolysis is the preferential energetic pathway driving the resorption activity of mature osteoclasts, whereas oxidative metabolism is also maintained to some extent, presumably to support other simultaneous cellular functions. This view is in line with the compartmentalization theory that postulates that different types of metabolic activities are localized and sequestered into different cellular compartments, according to the intracellular local needs. Therefore, we investigated the cellular localization of glycolytic enzymes in osteoclasts that are forming actin-ring structures that are needed for bone resorption. Although in fully differentiated osteoclasts we observed a signal for PKM2 and GAPDH glycolytic enzymes that spread from the cellular central main body throughout the cytoplasm, we also visualized a clear localisation in close proximity to the actin-ring structures (Fig. 7, white

arrows). Indeed, PKM2 and GAPDH also formed a ring-like structure. These results suggest that the glycolytic pathway localised at the site of actin ring formation energetically fuels the process of actin polymerisation.

Discussion

The results obtained in this study confirmed the presence of abundant mitochondria in human osteoclasts and a significant increase of the mitochondria content during the differentiation process, as already shown in other species (Ishii et al. , 2009, Wei et al. , 2010, Zeng et al. , 2015, Zhou et al. , 2013). Mitochondria in mature osteoclasts were increased in size and rich in cristae, especially when compared with their monocytic precursors. Likewise, very recent reports have shown a considerable structural remodelling of mitochondria during osteoclastogenesis of murine precursors (Zeng et al. , 2015). Furthermore, we observed the formation of a complex reticulum with mitochondrial networks spreading throughout the cells, from the perinuclear region to the peripheral basal domain, with organized, ramified and interconnected tubular structures. The formation of mitochondrial clusters around the nuclei is possibly crucial to efficiently fuel biosynthetic functions, whereas the complex reticulum at the basal domain might be needed for generating ATP at the peripheral regions of the cell. Interestingly, a steady increase in mtDNA content has been observed during the fusion of other cell types, like myoblasts (Frangini et al. , 2013). The expansion of mtDNA copy number is contextual to the increase of mitochondrial mass.

Mitochondrogenesis is usually associated with the expression OxPhos enzymes (Ishii et al. , 2009), and membranes decorated with cristae are the principal sites of OxPhos (Gilkerson et al. , 2003), whereas mitochondrial networks are important for generating ATP in the different districts of the cell (Archer, 2013). Therefore, it is likely that, based on our

morphological observation, OxPhos is the main metabolic pathway driving energy production during the osteoclast differentiation process and in fully differentiated osteoclasts. In agreement with this hypothesis, in murine monocytes undergoing osteoclast formation, the TCA cycle and oxidative phosphorylation are upregulated (Czupalla et al. , 2005). Consistently, by directly measuring the metabolic activity of live human cells, we found that osteoclasts present high levels of mitochondrial OCR and a low glycolytic efficiency. Conversely, in immature cells, we found a higher glycolytic efficiency, which usually occurs when all the glucose is converted into lactate, bypassing other metabolic pathways that utilize glucose or its metabolites (Zancan et al. 2010). In line with these results, in fully differentiated osteoclasts we demonstrated an increased expression of the prevalent complexes of the respiratory chain and a high intracellular ATP content. These data provide consistent evidence that mature osteoclasts rely on OxPhos for energy production to support the biosynthesis of the components demanded for differentiation. An increase in the expression of the enzymes of the respiratory chain parallels an increased expression of TCA cycle enzymes (Czupalla et al., 2005). Notably, despite the fact that results obtained with primary cell cultures of human osteoclasts are usually characterized by a huge variability, we found considerable reproducibility, thereby strongly supporting our conclusions. The fundamental role of mitochondriogenesis in osteoclast formation has been also recently indirectly demonstrated in a knockout animal model for transcription factor RelB of the NFkB pathway that is needed to propagate the signal for differentiation and function of osteoclasts (Zeng et al., 2015). Osteoclasts isolated from this model showed a reduced number of mitochondria with abnormal OxPhos enzymatic activities. In line with our results, RelB- murine osteoclasts also appeared to have a reduced number of cristae (Zeng et al., 2015). Similarly, other studies showed that normal mitochondrial function suppresses macrophage activation and inflammation while

promoting osteoclast differentiation (Jin et al., 2014). Indeed, M1 macrophages and dendritic cells that derive from the same osteoclast precursors are purely glycolytic cells (Loftus and Finlay, 2016). Furthermore, in the tumor murine model of osteoclasts RAW264.7 high levels of extracellular glucose strongly inhibit osteoclast differentiation. In an opposite fashion, pyruvate preferentially used by OxPhos, leads to a metabolic shift from glycolysis toward OxPhos, thereby promoting osteoclast differentiation (Kim et al., 2007).

Based on these and our observations, we conclude that mature osteoclasts are in a high energetic-state sustained by mitochondrial metabolism that might support most high energy-consuming functions, including bone resorption. To gain insights into the metabolic pathway that fuels osteoclast activity, we adjusted media composition with different metabolites, i.e. glucose or galactose as energy sources. Glucose is the natural substrate of glycolysis, whereas the oxidation of galactose to pyruvate through glycolysis yields no net production of ATP, inducing cells to rely on OxPhos to produce energy (Rossignol et al. , 2004). In both cases, with the addition of glucose or galactose, we found that osteoclasts preferentially resorb Type I collagen when they can use a functional glycolytic pathway. Consistently, under the same conditions, the addition of Complex I inhibitor rotenone did not impair osteoclast activity: rather, collagen degradation was induced. This effect was not due to cellular cytotoxicity, since we used a low dose of rotenone that does not alter cell viability. Our data on the regulatory effects of glucose on osteoclast activity are consistent with a previous report showing that at physiological concentrations glucose regulates bone resorption of chicken osteoclasts (Williams et al., 1997). However, it is not clear to date if glycolysis activation represents a whole cellular metabolic switch or if OxPhos is still active to support other cellular functions during bone resorption. What is clear from previous studies is that overexpression of PPar γ cofactor 1 β (PGC-1 β), a

positive regulator of mitochondrial biogenesis, does not further increase bone resorption even when OxPhos expression and mitochondrial mass increase (Zeng et al. , 2015).

Notably, hypoxia reduces the viability of mature osteoclasts, thereby suggesting that OxPhos supports osteoclast survival (Arnett, 2010, Knowles and Athanasou, 2009).

The theory of metabolic pathway compartmentalization is still in its infancy, partly due to the limited availability of methods to study the directionality of metabolic pathways and to visualize metabolic processes in distinct cellular compartments. However, in the case of complex cells bearing different cellular activities simultaneously operating at different subcellular regions as for osteoclasts (i.e. bone resorption, cytoskeleton reorganisation, vesicle trafficking, protein synthesis), the idea that metabolic enzymes are sequestered in different areas of the cells is particularly appealing. One of the major examples of metabolic compartmentalisation is the association of glycolytic enzymes with the actin cytoskeleton. For angiogenic endothelial cells, glycolytic enzymes compartmentalize in lamellipodia and filopodia to allow a rapid generation of ATP during the high-energy consuming processes of cell motility (De Bock et al., 2013). With a similar mechanism, during the energy-consuming process of bone resorption, osteoclasts undergo profound changes in the organization of microfilaments (Lakkakorpi and Vaananen, 1996). This occurs through the formation of podosomes, dynamic and self-organizing actin-based structures that are densely packed into a thick ring called the sealing zone (Touaitahuata et al. , 2013). We therefore speculated that local glycolysis allows a rapid generation of ATP for dynamic motility, and prevents taxing ATP demands through the cells. As a confirmation of our hypothesis, we found that PKM2 and GAPDH, two key enzymes of glycolysis, are localised very close to the F-actin structures that form the so-called actin-ring in multinucleated osteoclasts.

The compartmentalisation of glycolytic enzymes at the sealing zone might have other important implications. To reach a local pH around 4.7 in the resorption lacunae (Silver et al., 1988), an enormous proton release is exerted by the activity of the proton pump vacuolar ATP-ase (V-ATPase) at the ruffled border. The strong acidification at the resorption lacunae allows the dissolution of hydroxyapatite crystals and the digestion of organic bone matrix by acid proteases. Also in this case, the activity of V-ATPase is strictly dependent on the locally availability of large amounts of ATP (Cipriano et al., 2008, Francis et al., 2002, Qin et al., 2012). A direct coupling between the ATP-generating glycolytic enzymes and the ATP-hydrolyzing proton pump has already been demonstrated by the evidence that V-ATPase directly interacts with the A-subunit of phosphofructokinase-1 (Sun, 2012) and with the E-subunit of aldolase (Lu et al., 2001). Finally, the transport of vesicles to and from the ruffled border (Mulari et al. , 2003) is an additionally high energy consuming process that requires prompt and local energy. An example is offered by neurons in which the energy demand for fast axon transport of vesicles to nerve terminals and ion pumps is fulfilled by local glycolysis (Wu et al. , 1997, Zala et al., 2013).

In conclusion, in this study, we deeply investigated on osteoclast metabolism during their differentiation and activity. As already observed in rodent models, we confirmed in human osteoclasts that an increased mitochondrial mass and a high OxPhos are coupled to osteoclastogenesis. In addition, for the first time, we demonstrated that glycolysis drives osteoclast activity and is localized at subcellular level, close to the sealing zone. The coordination and spatial organisation between these metabolic pathways allows a perfect balance from mature osteoclast formation to the acquisition of bone resorption capacity. Understanding the coordination of bioenergetics in human osteoclast differentiation and function and a deeper characterization of compartmentalized metabolism in osteoclasts

may provide the basis for therapies to target osteolytic pathological process, like osteoporosis or bone metastases.

Acknowledgment

Author contributions: study conception (SA), work design (SL, PS, SA), data collection (SL, MS, PEP, NZ), analysis and interpretation of data (SL, PS, SA), drafting of manuscript (SL, NB, SA), critical revision (SL, MS, PS, GDP, NB, SA). This work was supported by the Italian Association for Cancer Research (AIRC MFAG to SA n. 14191), financial support for Scientific Research “5 per 1000 2012” to NB, and by Starting Grant from the European Research Council (ERC n. 243188 TUMETABO), the Belgian F.R.S.-FNRS, Interuniversity Attraction Pole (IAP) grant #UP7-03 from the Belgian Science Policy Office (Belspo) and an Action de Recherche Concertée from the Communauté Française de Belgique (ARC 14/19-058) to PS. Funding sources had no rules in study design, conducting the research, data analysis, preparation of the article, or decision to submit the article for publication. We thank Margherita Cortini for proof reading the article and MariaPia Cumani for the support to the graphical work.

Conflict of interest

The authors declare no competing financial interest.

References

- Archer, S.L., 2013. Mitochondrial dynamics--mitochondrial fission and fusion in human diseases. *N. Engl. J. Med.* 369, 2236-2251. 10.1056/NEJMra1215233.
- Arnett, T.R., 2010. Acidosis, hypoxia and bone. *Arch. Biochem. Biophys.* 503, 103-109. 10.1016/j.abb.2010.07.021.

- Avnet, S., Longhi, A., Salerno, M., Halleen, J.M., Perut, F., Granchi, D., Ferrari, S., Bertoni, F., Giunti, A., Baldini, N., 2008. Increased osteoclast activity is associated with aggressiveness of osteosarcoma. *Int. J. Oncol.* 33, 1231-1238.
- Avnet, S., Salerno, M., Zini, N., Alberghini, M., Gibellini, D., Baldini, N., 2013. Sustained autocrine induction and impaired negative feedback of osteoclastogenesis in CD14(+) cells of giant cell tumor of bone. *Am. J. Pathol.* 182, 1357-1366.
10.1016/j.ajpath.2012.12.021.
- Baron, R., Neff, L., Tran Van, P., Nefussi, J.R., Vignery, A., 1986. Kinetic and cytochemical identification of osteoclast precursors and their differentiation into multinucleated osteoclasts. *Am. J. Pathol.* 122, 363-378.
- Blair, J.M., Zheng, Y., Dunstan, C.R., 2007. RANK ligand. *Int. J. Biochem. Cell. Biol.* 39, 1077-1081. 10.1016/j.biocel.2006.11.008.
- Boyle, W.J., Simonet, W.S., Lacey, D.L., 2003. Osteoclast differentiation and activation. *Nature.* 423, 337-342. 10.1038/nature01658.
- Cenni, E., Perut, F., Granchi, D., Amato, I., Avnet, S., Brandi, M.L., Giunti, A., Baldini, N., 2006. Primitive and bone metastatic renal carcinoma cells promote osteoclastogenesis through endothelial cells. *Anticancer Res.* 26, 3065-3069.
- Cipriano, D.J., Wang, Y., Bond, S., Hinton, A., Jefferies, K.C., Qi, J., Forgac, M., 2008. Structure and regulation of the vacuolar ATPases. *Biochim. Biophys. Acta.* 1777, 599-604. 10.1016/j.bbabbio.2008.03.013.
- Czupalla, C., Mansukoski, H., Pursche, T., Krause, E., Hoflack, B., 2005. Comparative study of protein and mRNA expression during osteoclastogenesis. *Proteomics.* 5, 3868-3875. 10.1002/pmic.200402059.
- De Bock, K., Georgiadou, M., Schoors, S., Kuchnio, A., Wong, B.W., Cantelmo, A.R., Quaegebeur, A., Ghesquiere, B., Cauwenberghs, S., Eelen, G., Phng, L.K., Betz, I., Tembuyser, B., Brepoels, K., Welti, J., Geudens, I., Segura, I., Cruys, B., Bifari, F., Decimo, I., Blanco, R., Wyns, S., Vangindertael, J., Rocha, S., Collins, R.T., Munck, S., Daelemans, D., Imamura, H., Devlieger, R., Rider, M., Van Veldhoven, P.P.,

- Schuit, F., Bartrons, R., Hofkens, J., Fraisl, P., Telang, S., Deberardinis, R.J., Schoonjans, L., Vinckier, S., Chesney, J., Gerhardt, H., Dewerchin, M., Carmeliet, P., 2013. Role of PFKFB3-driven glycolysis in vessel sprouting. *Cell*. 154, 651-663. 10.1016/j.cell.2013.06.037.
- Demetrius, L., 2006. Aging in mouse and human systems: a comparative study. *Ann. N. Y. Acad. Sci.* 1067, 66-82. 10.1196/annals.1354.010.
- Erzurumlu, Y., Kose, F.A., Gozen, O., Gozuacik, D., Toth, E.A., Ballar, P., 2013. A unique IBMPFD-related P97/VCP mutation with differential binding pattern and subcellular localization. *Int. J. Biochem. Cell. Biol.* 45, 773-782. 10.1016/j.biocel.2013.01.006.
- Francis, M.J., Lees, R.L., Trujillo, E., Martin-Vasallo, P., Heersche, J.N., Mobasher, A., 2002. ATPase pumps in osteoclasts and osteoblasts. *Int. J. Biochem. Cell. Biol.* 34, 459-476.
- Frangini, M., Franzolin, E., Chemello, F., Laveder, P., Romualdi, C., Bianchi, V., Rampazzo, C., 2013. Synthesis of mitochondrial DNA precursors during myogenesis, an analysis in purified C2C12 myotubes. *J. Biol. Chem.* 288, 5624-5635. 10.1074/jbc.M112.441147.
- Gilkerson, R.W., Selker, J.M., Capaldi, R.A., 2003. The cristal membrane of mitochondria is the principal site of oxidative phosphorylation. *FEBS Lett.* 546, 355-358.
- Granchi, D., Amato, I., Battistelli, L., Avnet, S., Capaccioli, S., Papucci, L., Donnini, M., Pellacani, A., Brandi, M.L., Giunti, A., Baldini, N., 2004. In vitro blockade of receptor activator of nuclear factor-kappaB ligand prevents osteoclastogenesis induced by neuroblastoma cells. *Int. J. Cancer.* 111, 829-838. 10.1002/ijc.20308.
- Granchi, D., Amato, I., Battistelli, L., Ciapetti, G., Pagani, S., Avnet, S., Baldini, N., Giunti, A., 2005. Molecular basis of osteoclastogenesis induced by osteoblasts exposed to wear particles. *Biomaterials.* 26, 2371-2379. 10.1016/j.biomaterials.2004.07.045.
- Indo, Y., Takeshita, S., Ishii, K.A., Hoshii, T., Aburatani, H., Hirao, A., Ikeda, K., 2013. Metabolic regulation of osteoclast differentiation and function. *J. Bone Miner. Res.* 28, 2392-2399. 10.1002/jbmr.1976.

- Ishii, K.A., Fumoto, T., Iwai, K., Takeshita, S., Ito, M., Shimohata, N., Aburatani, H., Taketani, S., Lelliott, C.J., Vidal-Puig, A., Ikeda, K., 2009. Coordination of PGC-1beta and iron uptake in mitochondrial biogenesis and osteoclast activation. *Nat. Med.* 15, 259-266. 10.1038/nm.1910.
- Jin, Z., Wei, W., Yang, M., Du, Y., Wan, Y., 2014. Mitochondrial complex I activity suppresses inflammation and enhances bone resorption by shifting macrophage-osteoclast polarization. *Cell Metab.* 20, 483-498. 10.1016/j.cmet.2014.07.011.
- Kase, E.T., Nikolic, N., Bakke, S.S., Bogen, K.K., Aas, V., Thoresen, G.H., Rustan, A.C., 2013. Remodeling of oxidative energy metabolism by galactose improves glucose handling and metabolic switching in human skeletal muscle cells. *PLoS One.* 8, e59972. 10.1371/journal.pone.0059972.
- Kim, J.M., Jeong, D., Kang, H.K., Jung, S.Y., Kang, S.S., Min, B.M., 2007. Osteoclast precursors display dynamic metabolic shifts toward accelerated glucose metabolism at an early stage of RANKL-stimulated osteoclast differentiation. *Cell. Physiol. Biochem.* 20, 935-946. 10.1159/000110454.
- Knowles, H.J., Athanasou, N.A., 2009. Acute hypoxia and osteoclast activity: a balance between enhanced resorption and increased apoptosis. *J. Pathol.* 218, 256-264. 10.1002/path.2534.
- Knowles, H.J., Cleton-Jansen, A.M., Korsching, E., Athanasou, N.A., 2010. Hypoxia-inducible factor regulates osteoclast-mediated bone resorption: role of angiopoietin-like 4. *FASEB J.* 24, 4648-4659. 10.1096/fj.10-162230.
- Komarova, S.V., Ataulakhanov, F.I., Globus, R.K., 2000. Bioenergetics and mitochondrial transmembrane potential during differentiation of cultured osteoblasts. *Am. J. Physiol. Cell. Physiol.* 279, C1220-1229.
- Lakkakorpi, P.T., Vaananen, H.K., 1996. Cytoskeletal changes in osteoclasts during the resorption cycle. *Microsc. Res. Tech.* 33, 171-181. 10.1002/(SICI)1097-0029(19960201)33:2<171::AID-JEMT7>3.0.CO;2-W.

- Loftus, R.M., Finlay, D.K., 2016. Immunometabolism: Cellular Metabolism Turns Immune Regulator. *J. Biol. Chem.* 291, 1-10. 10.1074/jbc.R115.693903.
- Lu, M., Holliday, L.S., Zhang, L., Dunn, W.A., Jr., Gluck, S.L., 2001. Interaction between aldolase and vacuolar H⁺-ATPase: evidence for direct coupling of glycolysis to the ATP-hydrolyzing proton pump. *J. Biol. Chem.* 276, 30407-30413. 10.1074/jbc.M008768200.
- Massey, H.M., Flanagan, A.M., 1999. Human osteoclasts derive from CD14-positive monocytes. *Br. J. Haematol.* 106, 167-170.
- Miyazaki, T., Iwasawa, M., Nakashima, T., Mori, S., Shigemoto, K., Nakamura, H., Katagiri, H., Takayanagi, H., Tanaka, S., 2012. Intracellular and extracellular ATP coordinately regulate the inverse correlation between osteoclast survival and bone resorption. *J. Biol. Chem.* 287, 37808-37823. 10.1074/jbc.M112.385369.
- Morrison, M.S., Turin, L., King, B.F., Burnstock, G., Arnett, T.R., 1998. ATP is a potent stimulator of the activation and formation of rodent osteoclasts. *J. Physiol.* 511 (Pt 2), 495-500.
- Morten, K.J., Badder, L., Knowles, H.J., 2013. Differential regulation of HIF-mediated pathways increases mitochondrial metabolism and ATP production in hypoxic osteoclasts. *J. Pathol.* 229, 755-764. 10.1002/path.4159.
- Mulari, M.T., Zhao, H., Lakkakorpi, P.T., Vaananen, H.K., 2003. Osteoclast ruffled border has distinct subdomains for secretion and degraded matrix uptake. *Traffic.* 4, 113-125.
- Novack, D.V., 2011. Role of NF-kappaB in the skeleton. *Cell Res.* 21, 169-182. 10.1038/cr.2010.159.
- Pavlova, N.N., Thompson, C.B., 2016. The Emerging Hallmarks of Cancer Metabolism. *Cell. Metab.* 23, 27-47. 10.1016/j.cmet.2015.12.006.
- Qin, A., Cheng, T.S., Pavlos, N.J., Lin, Z., Dai, K.R., Zheng, M.H., 2012. V-ATPases in osteoclasts: structure, function and potential inhibitors of bone resorption. *Int. J. Biochem. Cell. Biol.* 44, 1422-1435. 10.1016/j.biocel.2012.05.014.

- Rossignol, R., Gilkerson, R., Aggeler, R., Yamagata, K., Remington, S.J., Capaldi, R.A., 2004. Energy substrate modulates mitochondrial structure and oxidative capacity in cancer cells. *Cancer Res.* 64, 985-993.
- Silver, I.A., Murrills, R.J., Etherington, D.J., 1988. Microelectrode studies on the acid microenvironment beneath adherent macrophages and osteoclasts. *Exp. Cell. Res.* 175, 266-276.
- Sun, S.C., 2012. The noncanonical NF-kappaB pathway. *Immunol. Rev.* 246, 125-140. 10.1111/j.1600-065X.2011.01088.x.
- Sweeney, S.E., Firestein, G.S., 2004. Rheumatoid arthritis: regulation of synovial inflammation. *Int. J. Biochem. Cell. Biol.* 36, 372-378.
- Teitelbaum, S.L., 2000. Bone resorption by osteoclasts. *Science.* 289, 1504-1508.
- Touaitahuata, H., Planus, E., Albiges-Rizo, C., Blangy, A., Pawlak, G., 2013. Podosomes are dispensable for osteoclast differentiation and migration. *Eur. J. Cell. Biol.* 92, 139-149. 10.1016/j.ejcb.2013.03.001.
- Utting, J.C., Flanagan, A.M., Brandao-Burch, A., Orriss, I.R., Arnett, T.R., 2010. Hypoxia stimulates osteoclast formation from human peripheral blood. *Cell. Biochem. Funct.* 28, 374-380. 10.1002/cbf.1660.
- Wei, W., Wang, X., Yang, M., Smith, L.C., Dechow, P.C., Sonoda, J., Evans, R.M., Wan, Y., 2010. PGC1beta mediates PPARgamma activation of osteoclastogenesis and rosiglitazone-induced bone loss. *Cell Metab.* 11, 503-516. 10.1016/j.cmet.2010.04.015.
- Weinberg, F., Hamanaka, R., Wheaton, W.W., Weinberg, S., Joseph, J., Lopez, M., Kalyanaraman, B., Mutlu, G.M., Budinger, G.R., Chandel, N.S., 2010. Mitochondrial metabolism and ROS generation are essential for Kras-mediated tumorigenicity. *Proc Natl. Acad. Sci. U. S. A.* 107, 8788-8793. 10.1073/pnas.1003428107.
- Williams, J.P., Blair, H.C., McDonald, J.M., McKenna, M.A., Jordan, S.E., Williford, J., Hardy, R.W., 1997. Regulation of osteoclastic bone resorption by glucose. *Biochem. Biophys. Res. Commun.* 235, 646-651. 10.1006/bbrc.1997.6795.

- Wu, K., Aoki, C., Elste, A., Rogalski-Wilk, A.A., Siekevitz, P., 1997. The synthesis of ATP by glycolytic enzymes in the postsynaptic density and the effect of endogenously generated nitric oxide. *Proc. Natl. Acad. Sci. U. S. A.* 94, 13273-13278.
- Zala, D., Hinckelmann, M.V., Yu, H., Lyra da Cunha, M.M., Liot, G., Cordelieres, F.P., Marco, S., Saudou, F., 2013. Vesicular glycolysis provides on-board energy for fast axonal transport. *Cell.* 152, 479-491. 10.1016/j.cell.2012.12.029.
- Zancan, P., Sola-Penna, M., Furtado, C.M., Da Silva, D, 2010. Differential expression of phosphofructokinase-1 isoforms correlates with the glycolytic efficiency of breast cancer cells. *Mol. Genet. Metab.*100, 372-378. doi: 10.1016/j.ymgme.2010.04.006
- Zeng, R., Faccio, R., Novack, D.V., 2015. Alternative NF-kappaB Regulates RANKL-Induced Osteoclast Differentiation and Mitochondrial Biogenesis via Independent Mechanisms. *J. Bone Miner. Res.* 30, 2287-2299. 10.1002/jbmr.2584.
- Zhou, J., Ye, S., Fujiwara, T., Manolagas, S.C., Zhao, H., 2013. Steap4 plays a critical role in osteoclastogenesis in vitro by regulating cellular iron/reactive oxygen species (ROS) levels and cAMP response element-binding protein (CREB) activation. *J. Biol. Chem.* 288, 30064-30074. 10.1074/jbc.M113.478750.
- Zini, N., Avnet, S., Ghisu, S., Maraldi, N.M., Squarzoni, S., Baldini, N., Lattanzi, G., 2008. Effects of prelamin A processing inhibitors on the differentiation and activity of human osteoclasts. *J. Cell. Biochem.* 105, 34-40. 10.1002/jcb.21796.

Figure Legend

Fig. 1. Mitochondrial mass increases during osteoclast differentiation. (A)

Representative images of TRAP and nuclear staining of osteoclast cultures at 2, 7 and 14 days (white arrows show multinucleated TRAP+ cells) and representative graph of the number of osteoclasts obtained at different end-points (n = 3). The trend was confirmed for 2 different donors; (B) Representative images of immunofluorescence with anti-mitochondria antibody (right panel) of osteoclast precursors at 2 days of culture (upper panel) and mature osteoclasts at 7 days of culture (bottom panel). The osteoclast phenotype of the observed cells was confirmed by TRAP staining and multinuclearity (left panel). Original magnification, 40x. Scale bar 20 μm ; (C) Mitochondrial mass index during osteoclastogenesis ($***p < 0.0001$, n=28); (D) Mitochondrial mass is directly correlated with the number of nuclei for cell ($R^2=0.9122$, n=9). Only cells with equal or more than 3 nuclei were considered; (E) Representative images of ultrastructural analysis of mitochondria from monocytic precursors (CD14+ cells) isolated from PBMC before seeding (upper panels) and mature osteoclasts (7 days, lower panels). Scale bars: 1.5-2 μm on the left, 0.2 μm on the right, 100 nm for magnification.

Fig. 2. Mitochondria of mature osteoclasts form tubular structures. Osteoclasts were

stained with an anti-mitochondria antibody, and analyzed by confocal microscopy. (A) Mature osteoclasts were identified by TRAP staining (grey in the white field) and the presence of 3 or more nuclei (by Hoechst staining). Mitochondria clustered in the perinuclear region (from the top and left panels to the bottom and right panels: merge image, blue channel, green channel, white field with grey colours, bar scale 20 μM); (B) Z-sections of one chosen scanned XY-section are also below (XZ-section), or on the right (YZ-section). White arrow shows tubular appearance of mitochondria towards the

peripheral basal domain. Representative image; (C) Volume render image of 20 optical sections, 0.18 μm thickness.

Fig. 3. Confocal analysis of immunofluorescence staining of mitochondria to reveal the mitochondria network in mature osteoclasts. Each XY-field of the 24 optical sections (0.18 μm thickness) are shown. White arrows show tubular appearance of mitochondria towards the peripheral basal domain.

Fig. 4. Expression of enzymes of the respiratory chain and total ATP intracellular content. (A) Immunoblot analysis of complex I (I-NDUFB8), complex II (II-SDHB), complex III (III-UQCRC2), complex IV (IV-COXII) and complex V (V-ATP5A) of the electron transport chain of osteoclasts (+RANKL/M-CSF) and immature cells (-RANKL/M-CSF). HSP60 immunoblot was used for normalization. Representative image; (B) Densitometric quantification of the signal detected in Western blot assays (ratio of each protein:HSP60), mean \pm SE, * $p < 0.05$, $n = 4$; (C) Total intracellular ATP content of osteoclasts on plastic substrate. Results were normalized to total protein content, mean \pm SE, ** $p < 0.01$, $n = 10$. (D) Total intracellular ATP content of osteoclasts on dentin substrate. Results were normalized to total protein content, mean \pm SE, *** $p < 0.001$, $n = 10$.

Fig. 5. Energetic metabolism during osteoclast differentiation. Osteoclasts and immature cells were cultured for 14 days, and baseline ECAR and OCR were measured using the Seahorse Flux Analyzer. Typically, after the incubation with osteoclast differentiation factors (RANKL and M-CSF), osteoclasts are formed starting from day 7. ECAR, extracellular acidification rate; OCR, oxygen consumption rate; mtOCR, mitochondrial OCR. Graphs showed the ECAR (A) and OCR measurements (B) at

different time points of a representative osteoclast culture obtained from a single donor (A, B, C, D vertical lines correspond to the time of injection of oligomycin, FCCP, rotenone and antimycin A, 2-deoxy-glucose 100 mM respectively); (C) ECAR, mtOCR, and ATP coupling values of cells treated with osteoclast differentiating factors, or not treated, at 7 days of cultures. Average of different cultures obtained from three different donors. Mean \pm SE (* $p < 0.05$, $n = 3$); (D) Glycolytic efficiency (glucose consumption/lactate production ratio). Average of the different cultures obtained from 5 different donors. Data were expressed as percentages in respect to –RANKL/M-CSF condition. *** $p < 0.0001$, $n = 5$. All the results were normalized to total protein.

Fig. 6. The degradation of Type I collagen relies on glycolysis. (A) Type I Collagen degradation activity of osteoclasts cultured with medium enriched with either glucose or galactose, or with galactose supplemented with rotenone 10 nM. The values are expressed as percentage in respect to the condition of cells treated with galactose. Glucose *versus* galactose, * $p < 0.05$, $n = 5$, mean \pm SE; galactose *versus* galactose and rotenone, ** $p < 0.01$, $n = 8$, mean \pm SE. (B) The effect of different concentrations of rotenone in galactose media on cell viability was tested with Alamar Blue fluorescence. Results are normalized to total protein content, * $p < 0.05$, ** $p < 0.01$, $n = 6$. (C) The necrotic effect of different concentrations of rotenone in galactose media was tested by staining with propidium iodide nucleic acid binding dye. *** $p < 0.001$, $n = 8$.

Fig. 7. The glycolytic enzymes PKM2 and GAPDH localise at the sealing zone, close to the actin ring. Osteoclasts were stained with an anti-PKM2 or anti-GAPDH Alexafluor 488-antibodies (green) together with Falloidin-TRITC (red) to stain F-actin, and analyzed by confocal microscopy. The white arrows show the rings formed by PKM2 and GAPDH in

close proximity to the actin ring at the sealing zone. (A) xy section of osteoclasts forming the actin ring (left panel: merge image, right panel: green channel; bar scale 20 μM); (B) details of the sealing zone in XY-section (XZ-section), (left panel: merge image; middle panel: green channel; right panel: red channel, bar scale 10 μM); (C) Z-scans of an osteoclast stained for GAPDH (green) and F-actin (red). All XY-fields of the 16 optical sections (0.6 μm thickness) are shown.

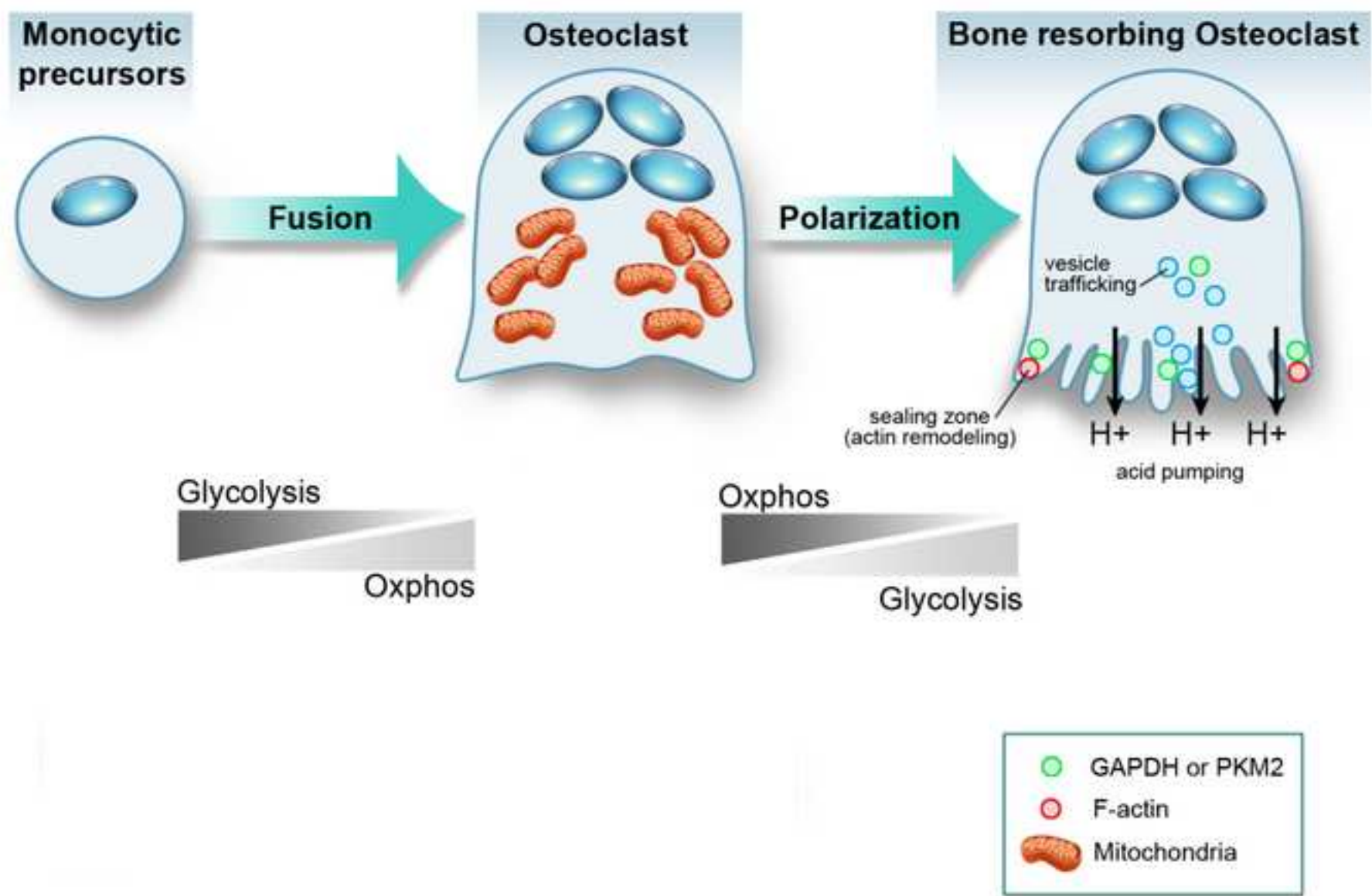


Figure 1 revised

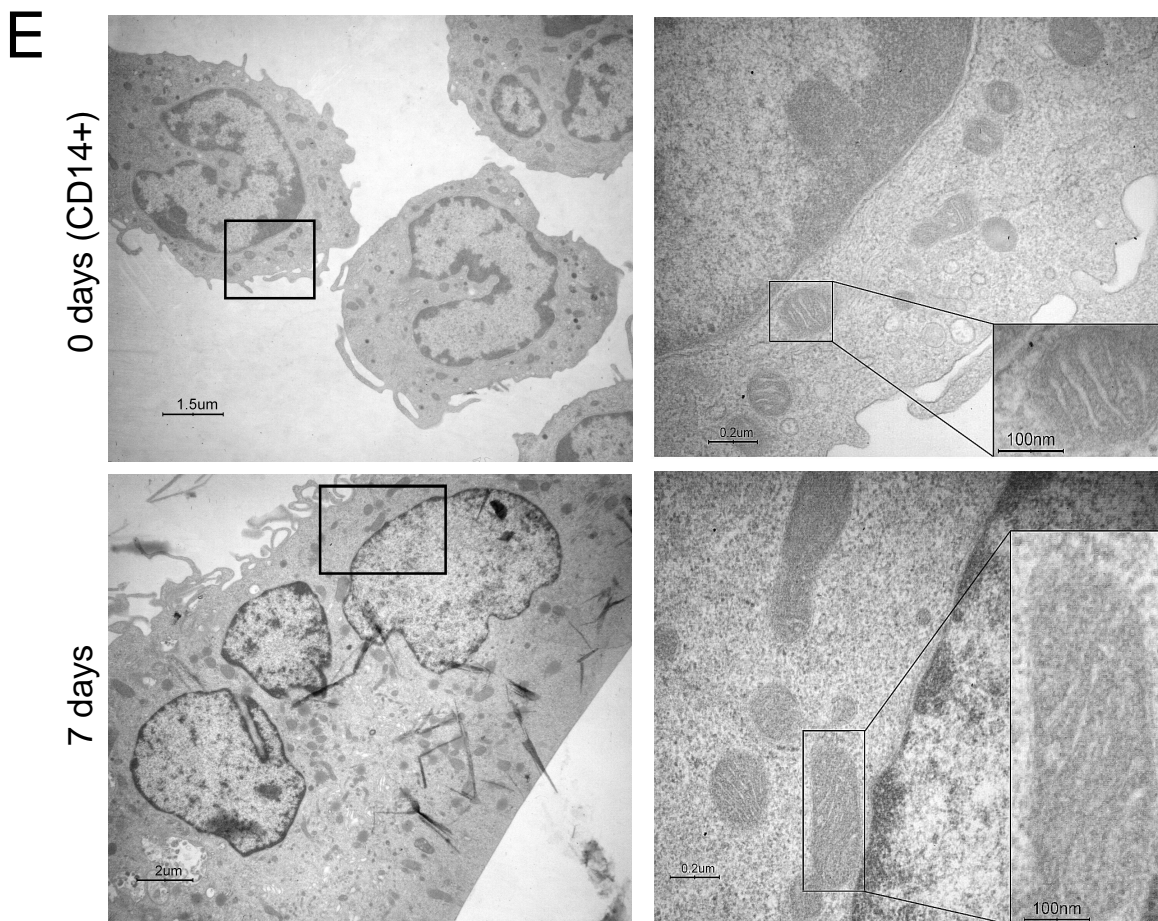
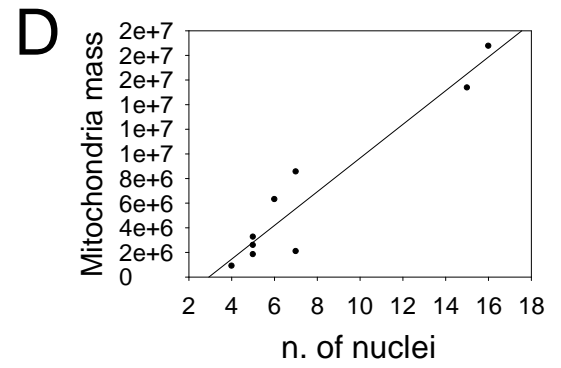
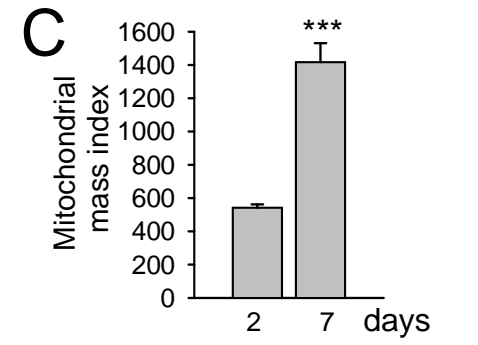
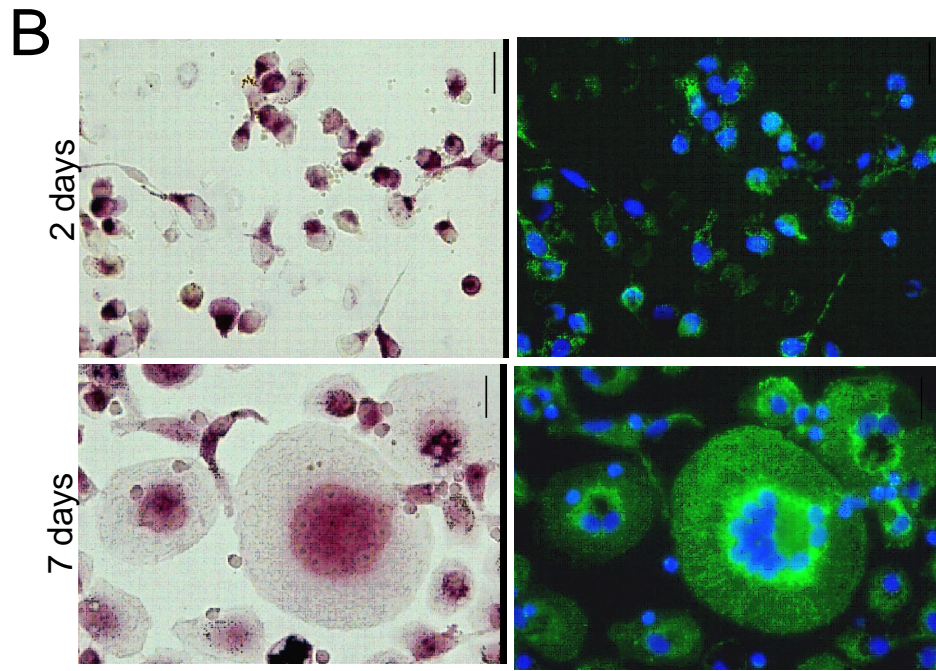
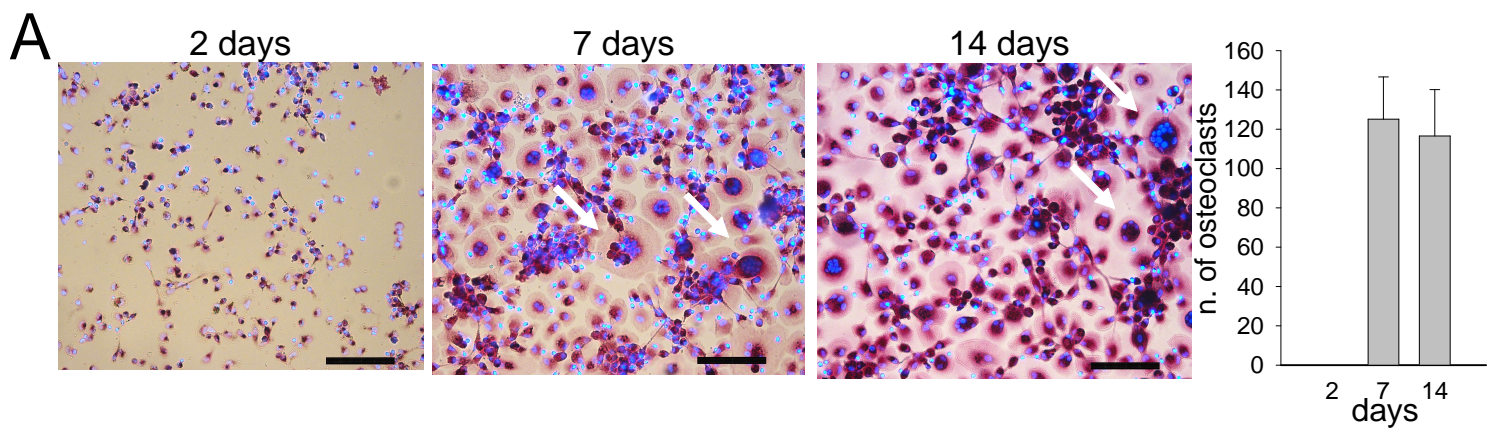
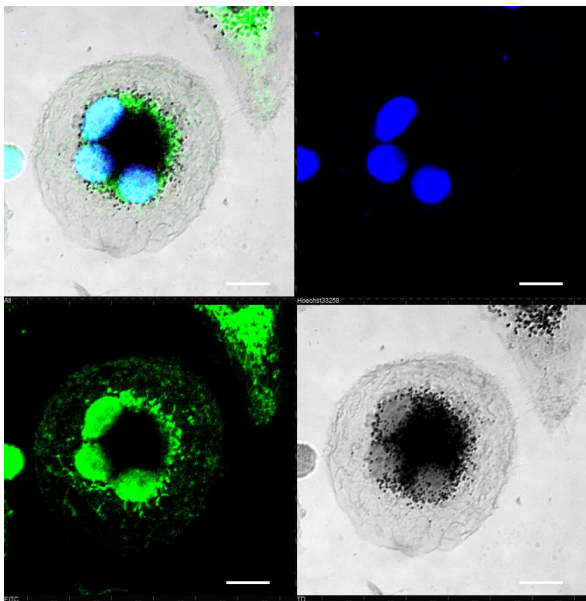
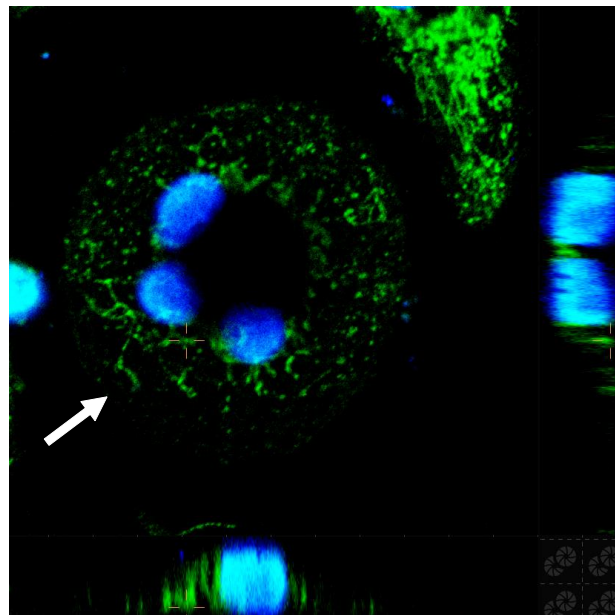


Figure 2 revised

A



B



C

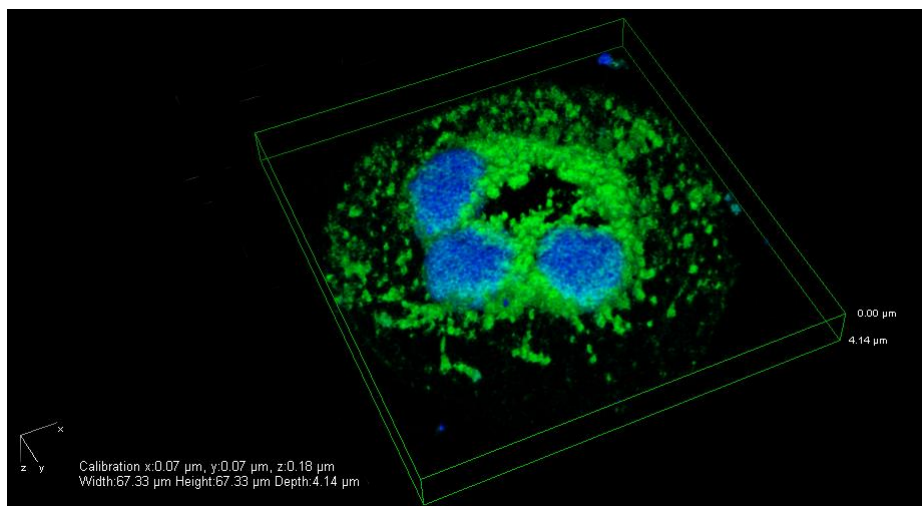


Figure 3 revised

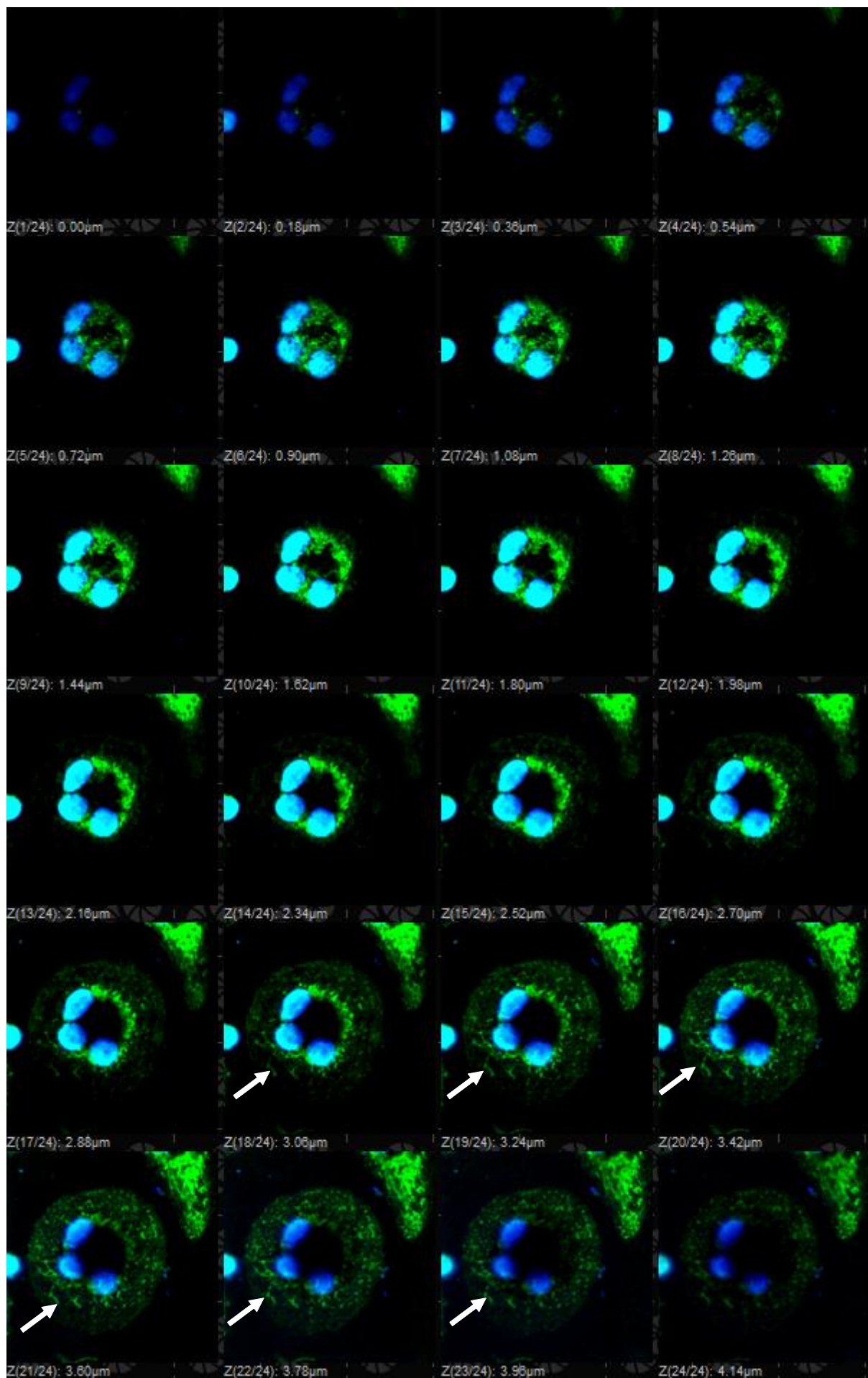


Figure 4 revised

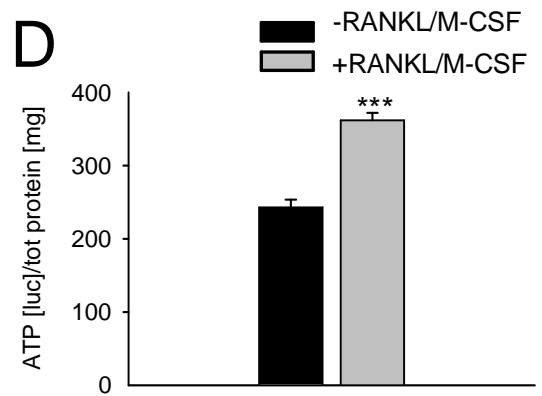
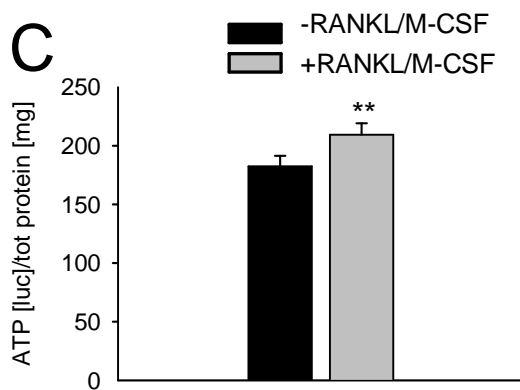
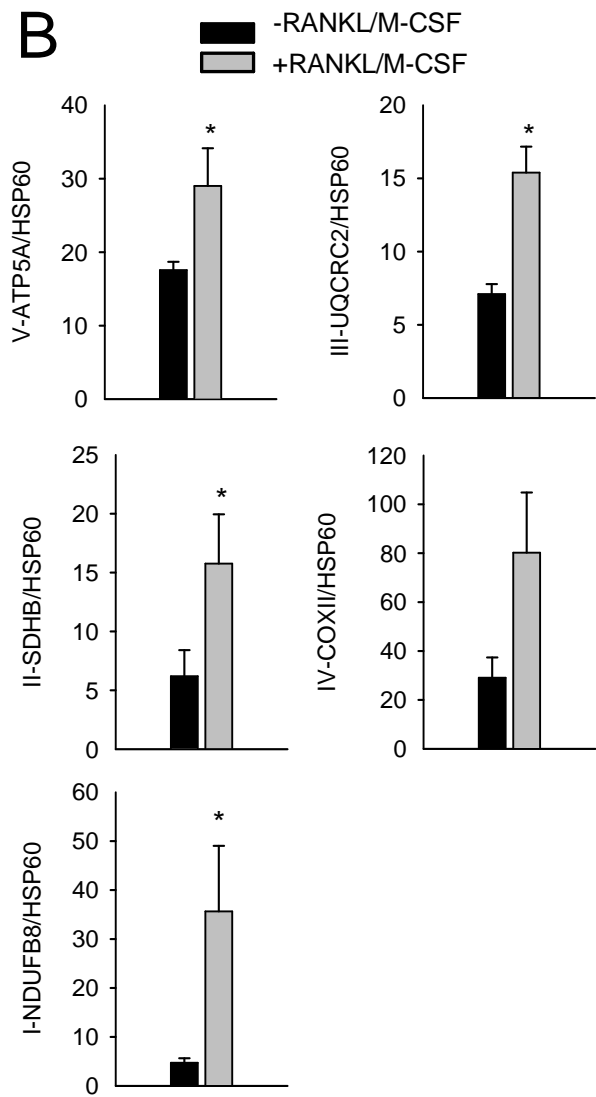
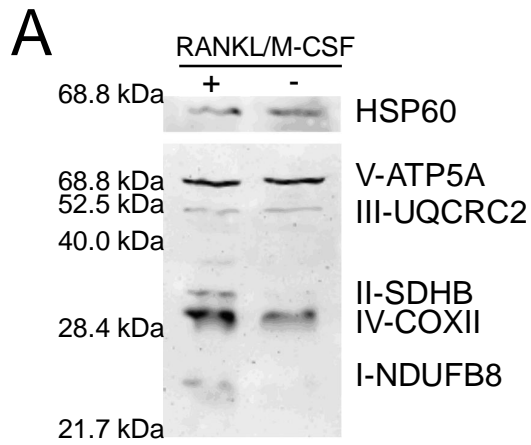
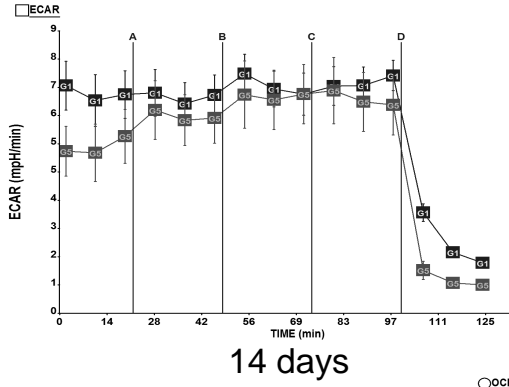
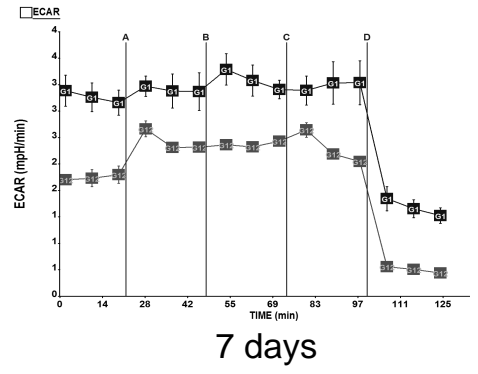
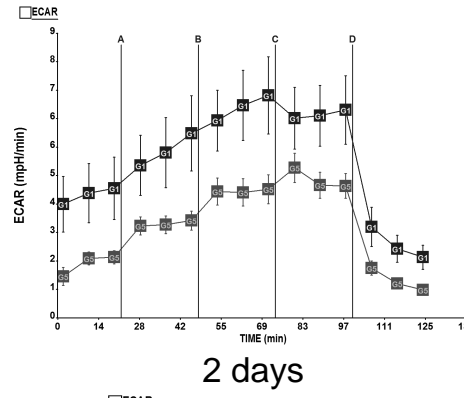


Figure 5 revised

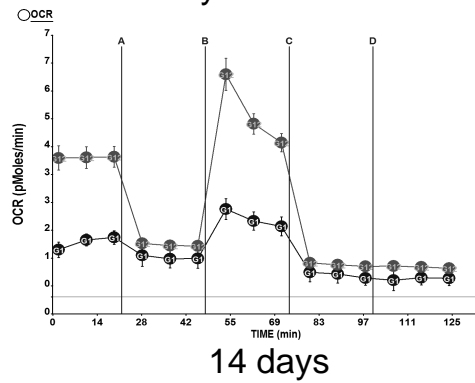
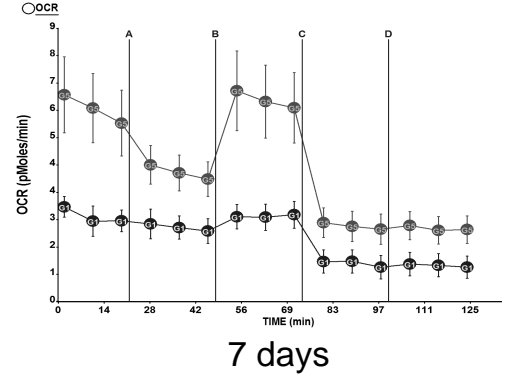
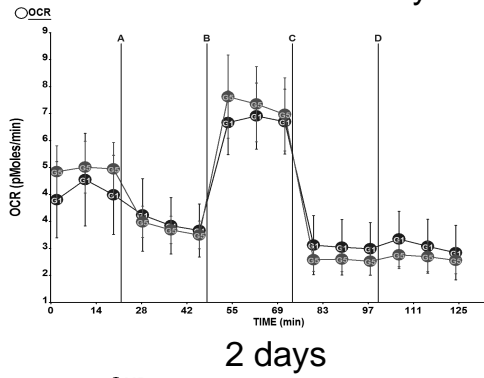
A

-RANKL/M-CSF
 +RANKL/M-CSF

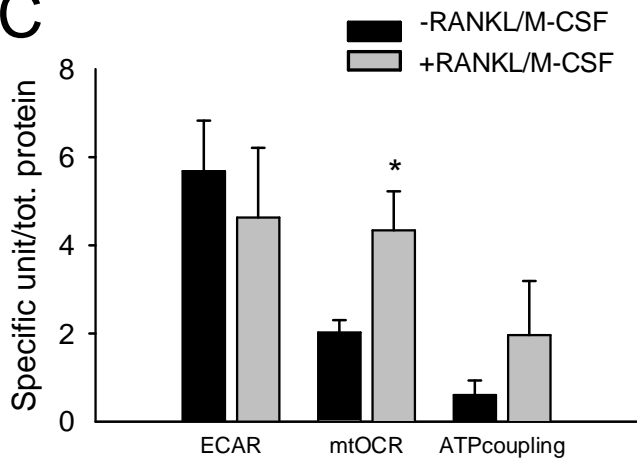


B

-RANKL/M-CSF
 +RANKL/M-CSF



C



D

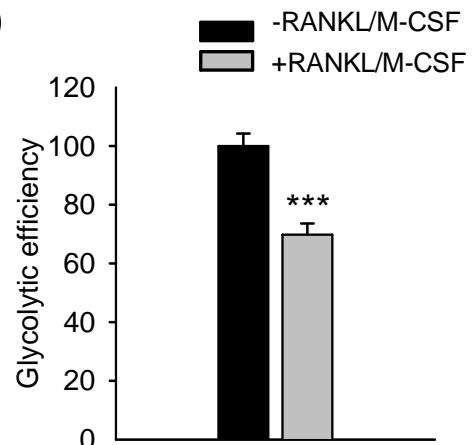
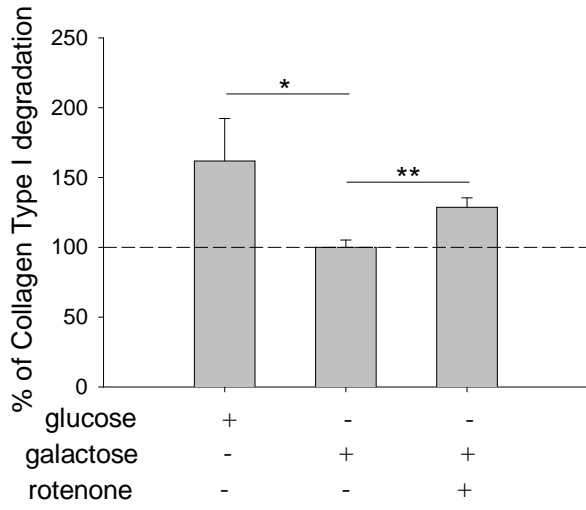
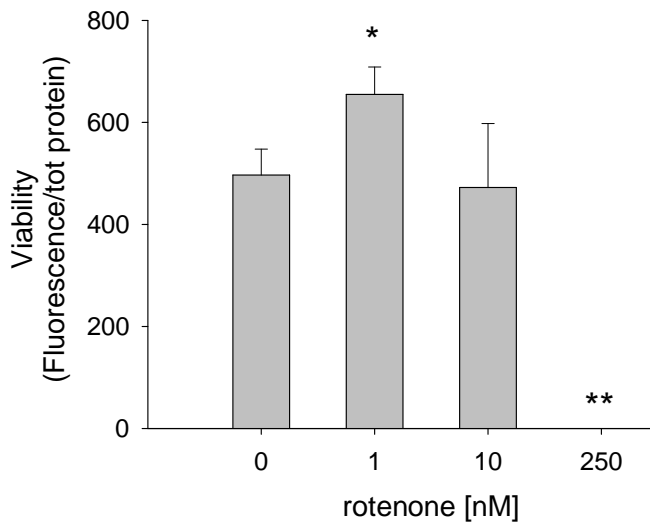


Figure 6 revised

A



B



C

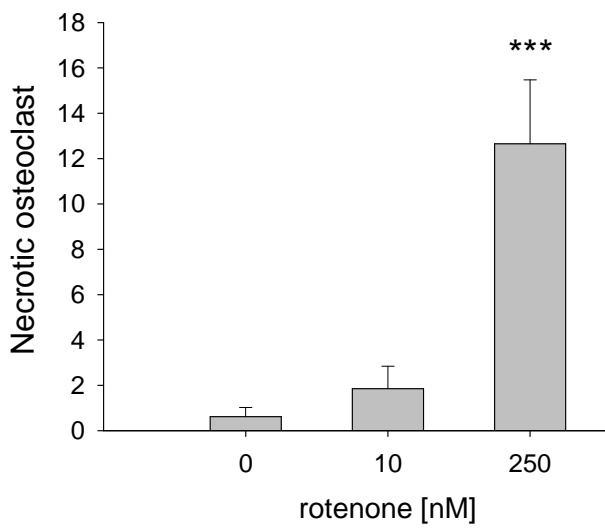
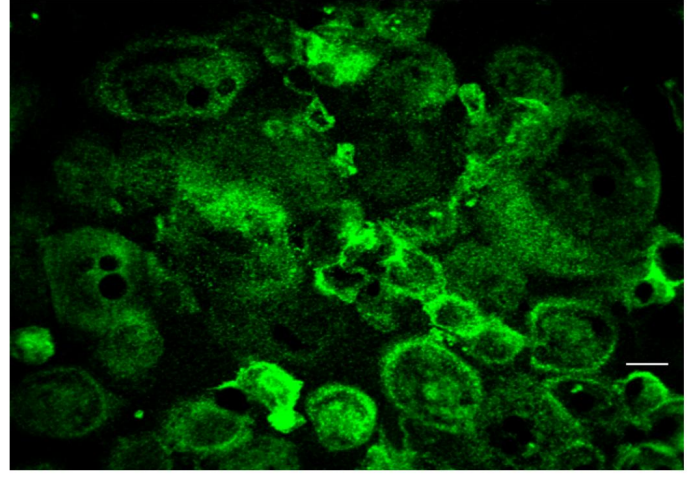
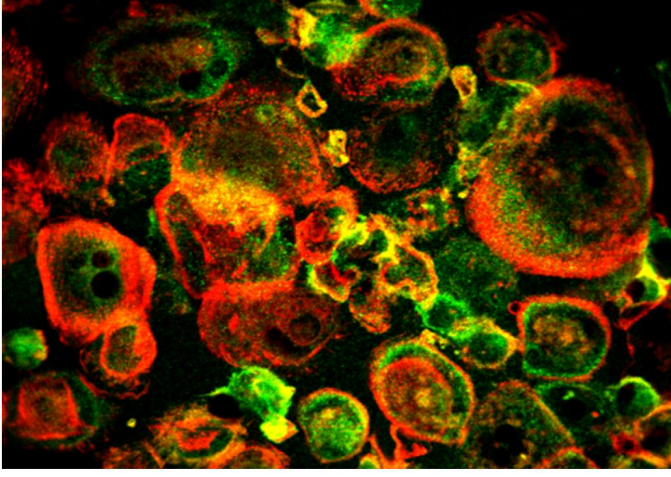


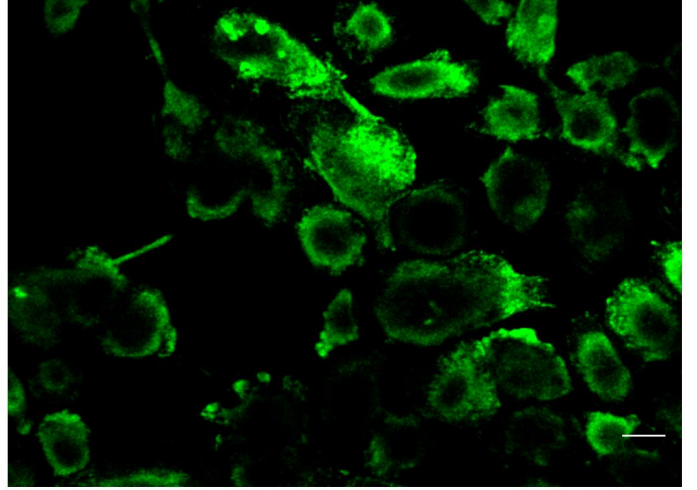
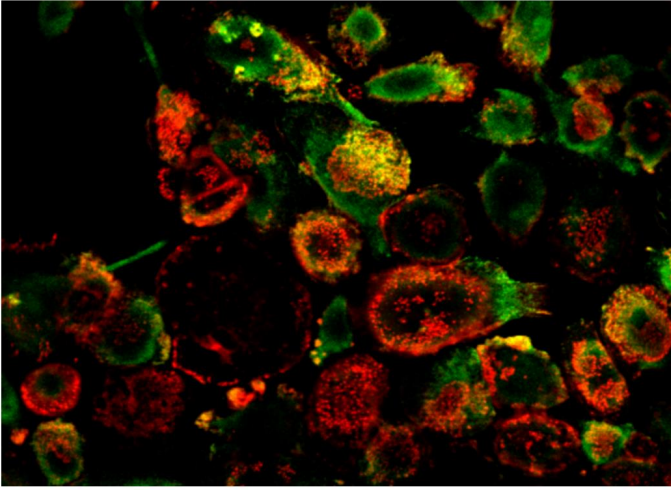
Figure 7

A

F-actin and GAPDH

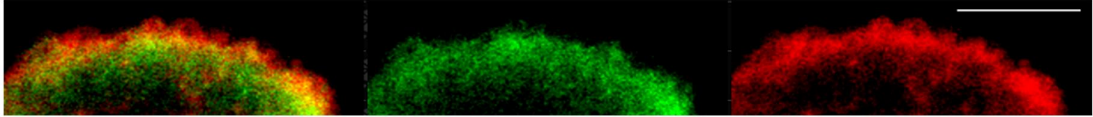


F-actin and PKM2

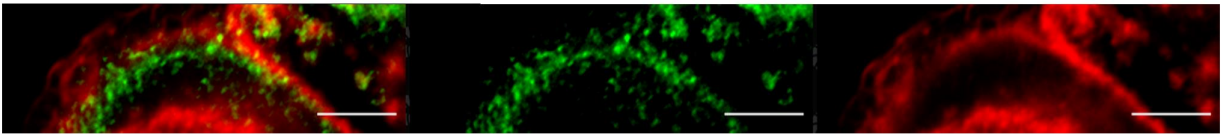


B

F-actin and GAPDH



F-actin and PKM2



C

F-actin and GAPDH

